Frequency-tunable and Circularly Polarized Microwave Resonator for Magnetic Sensing with NV Ensembles in Diamond

Heng Yuan, *Member, IEEE*, Xiaoying Yang, Ning Zhang,

Zhiqiang Han, Lixia Xu, Jixing Zhang, Guodong Bian, Pengcheng Fan, Mingxin Li, and Yuchen Liu

***Abstract*—A microwave (MW) resonator to provide frequency-tunable and circularly polarized MW fields is proposed. This technology enlarges the range of application in optically detected magnetic resonance (ODMR) systems based on the diamond negatively charged nitrogen-vacancy (NV) center and enable the selective excitation of its electronic spins. The characteristics of this resonator are simulated and discussed via a series of experimental studies. An adjustable MW frequency (f_{MW}) can be provided in the 2.5-3.1GHz range and the value of the input return loss (S_{11}) corresponding to f_{MW} measures < -15dB which mean at least 96.84% coupling efficiency between the microwave resonator and the microwave source. When f_{MW} is equal to the resonance frequency of the NV center (f_{NV}) for different external magnetic fields (*B*), the results of the ODMR experiment indicate that the fluorescence increases upon an increase in |*B*|. Finally, the resonator provides a circularly polarized MW output with a purity of 97.17%. This study paves the way to novel applications and to the development of magnetic sensing devices based on the NV ensemble in diamond.**

***Index Terms*—magnetic sensing, microwave field, circular polarization, microwave frequency, nitrogen-vacancy center**

I. Introduction

Magnetic field sensors have been widely applied in various fields such as military, navigation, medical and biological applications. [1] Hall effect based magnetic field sensors are easily built using mixed signal CMOS processes. Therefore, they are commonly used whenever there is need for a low cost magnetic field sensor with moderate performance.[2] Anisotropic magnetoresistive (AMR) sensors, giant magnetoresistive (GMR) sensors and spin-dependent tunneling (SDT) sensors have become standard off-the-shelf devices for use in medium-accuracy applications; fluxgate sensors measure DC and low-frequency AC fields up to approximately 1 mT with a resolution of 100 pT and with linearity-error less than 10 ppm. The best fluxgate magnetometers use a Compact Spherical Coil (CSC), and the disadvantages of CSC are as follows: large volume, high price and the sensors cannot be removed without breaking the coils.[3] Compared with traditional measurement methods, quantum sensors based on atomic spin resonance effect have become one of the most promising research in the field of sensing and measurement. The negatively charged nitrogen-vacancy (NV) center [4] in diamond is widely used in quantum sensing, [5], [6], in metrology applications [7]-[9] which require a high optical stability, [10], [11], in spin state manipulations via mi33crowaves (MWs), [12], [13], and in preserving quantum coherence at room temperature [14], [15]. In the domain of vector magnetic field sensing—ranging from DC to MW field—a sensitivity of up to sub-picotesla has been achieved using the NV center ensemble within an effective volume of sub-milliliter range. [16]-[19] Magnetic sensor based on spin ensembles of NV centers has great potential in applications involving miniaturization and integration, while its comprehensive performance is expected to be comparable with currently the recent most advanced superconducting quantum interference device (SQUID) magnetometer and vapor cell magnetometer [20]-[22].

The NV center has C_{3v} symmetry in the diamond crystal lattice, as is shown in Fig. 1(a). Since the number of active NV centers enhances the sensitivity of the measurements, NV ensembles are used for high-precision measurements [23], [24], [25] via a MW field within the NV ensembles plays a key role in the measurement of the magnetic field [26]. The NV spin manipulation techniques for improving the practicability of such sensors has drawn great attention. However, the spin state manipulation relies on an applied bias magnetic field provided by Helmholtz coils in general, which is difficult to reduce the volume of magnetic sensor. Aim at this problem, the spin transition selection rule, which states that electrons belonging to the $m_s = 0$ sublevel can be excited into $m_s = \pm 1$ sublevels by $\sigma^{\pm}$ circularly polarized MW fields, has been verified [27], [28], as shown in Fig. 1(b). This facilitates the study of spin state

This work was supported by the National Key R&D Program of China 2016YFB0501604; the Projects of National Natural Science Foundation of China under Grant No. 61773046, 11575062, and 11665004; the Projects of Beijing Academy of Quantum Information Sciences under Grant No. Y18G33, and the Advanced Innovation Center of Big Data Precision Medicine of Beihang University.

H. Yuan, X. Yang, Z. Han, L. Xu, J. Zhang, G. Bian, P. Fan, M. Li, and Y. Liu are with School of Instrumentation and Optoelectronic Engineering, Beihang University, Beijing 100191, China, and H. Yuan are also with Laboratory of Quantum Sensing Technology, Ministry of Industry and Information Technology, Beijing 100191, China (e-mail: ningzhang@zhejianglab.com; lyxying@buaa.edu.cn;).

N. Zhang is with Research Center for Quantum Sensing Zhejiang Lab, Hangzhou 310000, China.

This article has been accepted for publication in a future issue of this journal, but has not been fully edited. Content may change prior to final publication. Citation information: DOI 10.1109/JSEN.2020.2974275, IEEE Sensors Journal

manipulations within the NV without the influence of magnetic fields [29]. However, the major drawback of the currently used circularly polarized MW resonators is their narrow bandwidth [30]-[32], which influences the MW frequency (f_{MW}) when the near field couples to the adjacent components of the system [33]. Furthermore, the resonance frequency of the NV center (f_{NV}) changes when an external magnetic field, $\boldsymbol{B}$, is applied: this results in a mismatch between f_{NV} and f_{MW} [34]. The large frequency shift ($f_{MW} \neq f_{NV}$) brings out the off-resonance between the MW field and the ensembles, decreasing the variations in the fluorescence process. In serious cases, this will result in the magnetic sensor being unable to make magnetic measurements. Moreover, this phenomenon generates instabilities in the magnetic sensing system by introducing noise under the form of static magnetic fluctuations, mechanical vibrations, and thermal expansion [33].

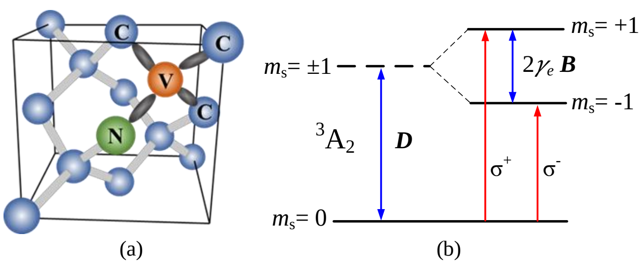

Fig.1. (a) The atomic structure of the NV center. (b) Energy levels of NV⁻ center and selective excitation of the circularly polarized MW field. The ground state of the NV center is an S = 1 spin triplet ($^3A_2$) with the $m_s = \pm1$ sublevels lying D = 2870 MHz above the $m_s = 0$ sublevel under zero magnetic field. An external magnetic field $\boldsymbol{B}$ split the $m_s = \pm1$ sublevels by $2\gamma_e\boldsymbol{B}$.

Aiming at the above problems, the main innovation of this work was proposed frequency-tunable and circularly polarized microwave resonator for magnetic sensing with NV ensembles in diamond. The MW provided by resonator can achieve frequency matching between f_{MW} and f_{NV}. Moreover, with this system, the S = 1 characteristic of the NV spin can be used to develop novel quantum sensing and metrology applications. The f_{MW} of the resonator is adjustable upon a change in the voltage. Moreover, the characteristics of the resonator are discussed via a series of experimental studies based on NV centers. The design of the frequency-tunable and circularly polarized resonator has important significance to miniaturization of magnetic sensor and advances the state of investigations on NV ensembles in diamond for quantum sensing in a wide range of magnetic resonance experiments.

II. Methods

A. Experimental Setup

The magnetic sensing system in Fig. 2 was built based on the optical polarization and detection properties of the NV centers. The performance of the resonator was tested via optically detected magnetic resonance (ODMR) [35] on the NV ensembles. The MW signal is generated via a MW signal generator with a maximum output power of +10 dBm. Moreover, the MW signal is split into two signals by employing a splitter. A programmable phase shifter is inserted in one of the electrical lines after the splitter to obtain two MW signals with a phase offset, Δφ. These two MW signals are connected to the port 2 and 3 of the resonator, respectively. The other two ports are connected to two 50 Ω terminators. The NV center ensemble generates a red fluorescence when the 532 nm green laser illuminates the diamond sample. The intensity of the red fluorescence is measured by using an avalanche photodiode to detect the electron spin ensemble population distribution. To obtain the maximum fluorescence contrast (F_{con}), the resonator frequency matching condition $f_{MW} = f_{NV}$ has to be obtained by adjusting the DC voltage source.

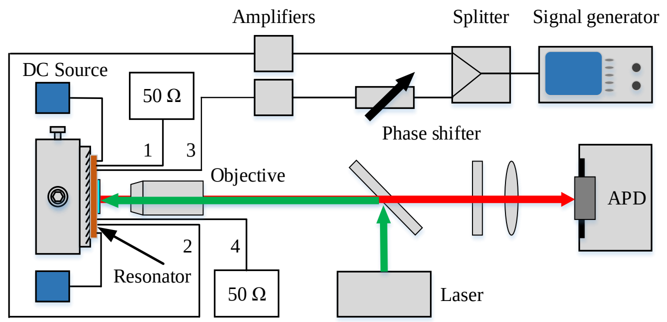

Fig.2. Schematic of the experimental system. The green and red lines represent the 532 nm green laser and the 637nm red fluorescence, respectively. The orange rectangle represents the resonator and both the two blue rectangles represent DC voltage sources. And the avalanche photodiode is defined APD in this figure. The DC source controls the varactor diodes to generate different f_{MW} in the resonator.

B. Resonator model

This resonator was built based on the results of a series of simulations using the High Frequency Structure Simulator (HFSS) software for printed circuit boards (PCB). Figure 3(a) and (b) show the photography of the resonator and a sketch with its dimensions, respectively. The varactor diodes C_1 and C_4 are controlled by a voltage, which is can be adjusted in the 0 ~15 V range by varying the direct current (DC) source I. The varactor diodes C_2 and C_3 are controlled via an identical mechanism by using the DC source II. The capacitance C_0 plays the role of a DC block in the resonator circuit. The resonator has four ports, named ports 1 ~ 4, to provide the circularly polarized MW field and impedance matching. Ports 2 and 3 are used to generate a phase difference to adjust the MW polarization, whereas the other two ports are connected to 50 Ω terminators.

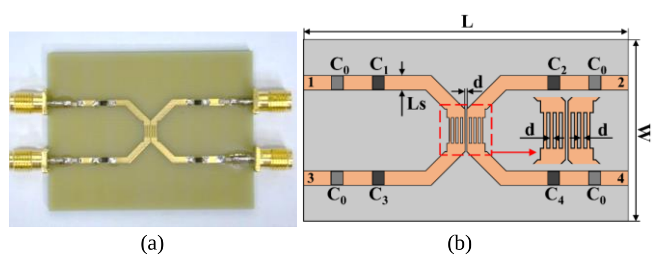

Fig.3. (a) Photograph of the proposed resonator; (b) Sketch of the resonator with its geometrical dimensions: The length of the resonator is L = 57 mm, the width of the resonator is W = 40mm, the width of the microstrip line are Ls = 3.7 mm, and d = 0.2mm. The capacitance measures C_0 = 10 pF (SN: ATC600S)

and the value of varactor diodes C_1–C_4 (SN: SMV1234) is 9.63 pF when no voltage is applied.

III. Results and Discussions

A. Frequency measurement

The adjustable DC voltage sources I and II regulate the value of the varactor diode to generate different f_{MW} and their corresponding input return loss (S_{11}). S_{11} represents the reflections induced in the system due to the impedance mismatch at the cable connection, and it can be expressed in a logarithmic form as follows:

$$S_{11} = -10 \mid \log_{10}(P_1 / P_2) \mid. \tag{1}$$

Where, P_1 and P_2 corresponds to the reflected wave power and the incident wave power, respectively. As shown in Fig. 4(a), which presents the measurements performed with a network analyzer, the f_{MW} and S_{11} values of the resonator change upon a variation in the voltage of the DC sources. Figure 4(b) and (c) show the variation range of f_{MW} and S_{11} upon a change in the voltage, respectively.

The f_{MW} can be adjusted in the 2.5~3.1 GHz range by changing the value of the DC sources. The network analyzer displays the S_{11} value corresponding to the f_{MW} of the designed resonator. The values of S_{11} corresponding to f_{MW} are all lower than -15 dB, implying that a minimal coupling efficiency of 96.84% between the microstrip antenna and the MW source can be achieved.

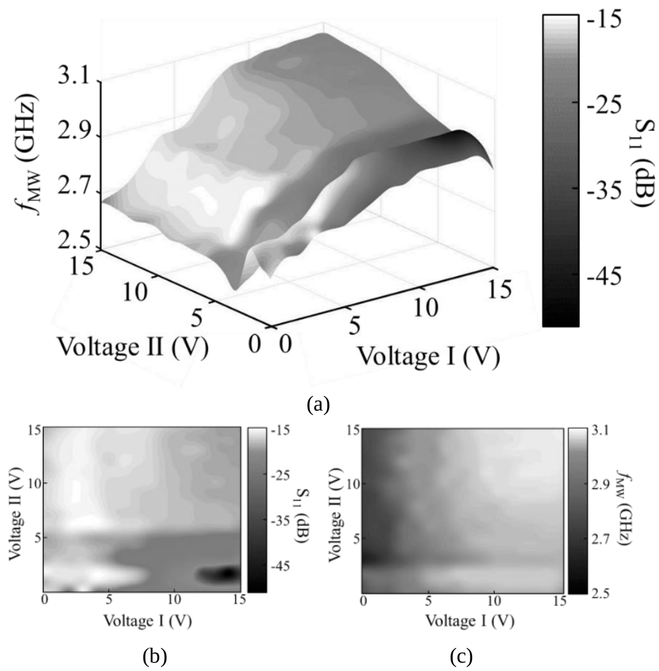

Fig.4. (a) Variation of f_{MW} and S_{11} of the resonator as a function of the voltages. The x-coordinate and the y-coordinate correspond to the voltage value of the DC source I and II, respectively. The z-coordinate corresponds to the f_{MW}. The color represents the value of S_{11} corresponding to f_{MW}. (b) Variation of f_{MW} as a function of the voltages. (c) Variation of S_{11} as a function of the voltages.

B. Frequency matching

The ground state electron spin sublevels ($m_s = \pm1$) of each NV center are subject to the Zeeman split in the presence of an applied magnetic field. The magnetic field $\boldsymbol{B}$ is applied along the [100] crystal axis and the magnetic field along the NV axis is indicated as $\boldsymbol{B_0}$. The value of f_{NV} can be adjusted via the applied magnetic field, $\boldsymbol{B_0}$, whereas different resonance frequencies, f_{MW}, are obtained by adjusting the values of the DC voltage sources. This results in the generation of frequencies in the spin levels of values $f_{NV} = D \pm \gamma \boldsymbol{B_0}$. The values of f_{NV} were extracted in ODMR experiment under different magnetic fields, and figure 5(a) shows the relation between f_{NV} (corresponding to $m_s = +1$) and the applied magnetic field, $\boldsymbol{B_0}$. Points are measured data and black line is fitting curve, and the fitting function is $f_{NV} = 2.798$ MHz/G × $\boldsymbol{B_0}$ + 2870 MHz.

To demonstrate that the resonator can provide frequency-tunable MW fields, f_{MW} was adjusted to match f_{NV} in the presence of different applied magnetic field during the ODMR experiment. The condition $m_s = +1$ corresponds to the resonance peak shifts induced by $\boldsymbol{B_0}$, as shown in Fig. 5(b). By sweeping of the applied magnetic field, $\boldsymbol{B_0}$, $m_s = +1$ corresponds to a change in F_{con}. Upon frequency matching ($f_{MW} = f_{NV}$), the changes in the fluorescence increase with the increase of $|\boldsymbol{B}|$. The value of changes in the fluorescence was extracted under different magnetic fields, and this changes upon a variation in $\boldsymbol{B_0}$, as reported in Fig. 5(c). The blue filled circles and the red filled squares represent the experimental values of F_{con} corresponding to $\boldsymbol{B_0}$ = -30 ~ -5G and $\boldsymbol{B_0}$ = +30 ~ +5G, respectively. The curves are fitted with Gaussian functions, and its expression is

$$F_{con} = \mathrm{a} \times e^{(-((B_0 - \mathrm{b})/\mathrm{c})^2} + d. \tag{2}$$

Here, a, b, c, and d are parameters.

The experimental results show the values of F_{con} increase upon an increase in $|\boldsymbol{B_0}|$ when f_{MW} matches f_{NV}. The f_{MW} of the designed resonator is adjustable and this implies that the NV ensemble works around the envelope peak. Moreover, the measurement accuracy for magnetic sensing with NV ensembles in diamond increases since the possibility of errors within the frequency range is decreased. Therefore, by calibrating f_{MW} to f_{NV}, the application scope of the microstrip resonator in a magnetic sensing system increases.

This article has been accepted for publication in a future issue of this journal, but has not been fully edited. Content may change prior to final publication. Citation information: DOI 10.1109/JSEN.2020.2974275, IEEE Sensors Journal

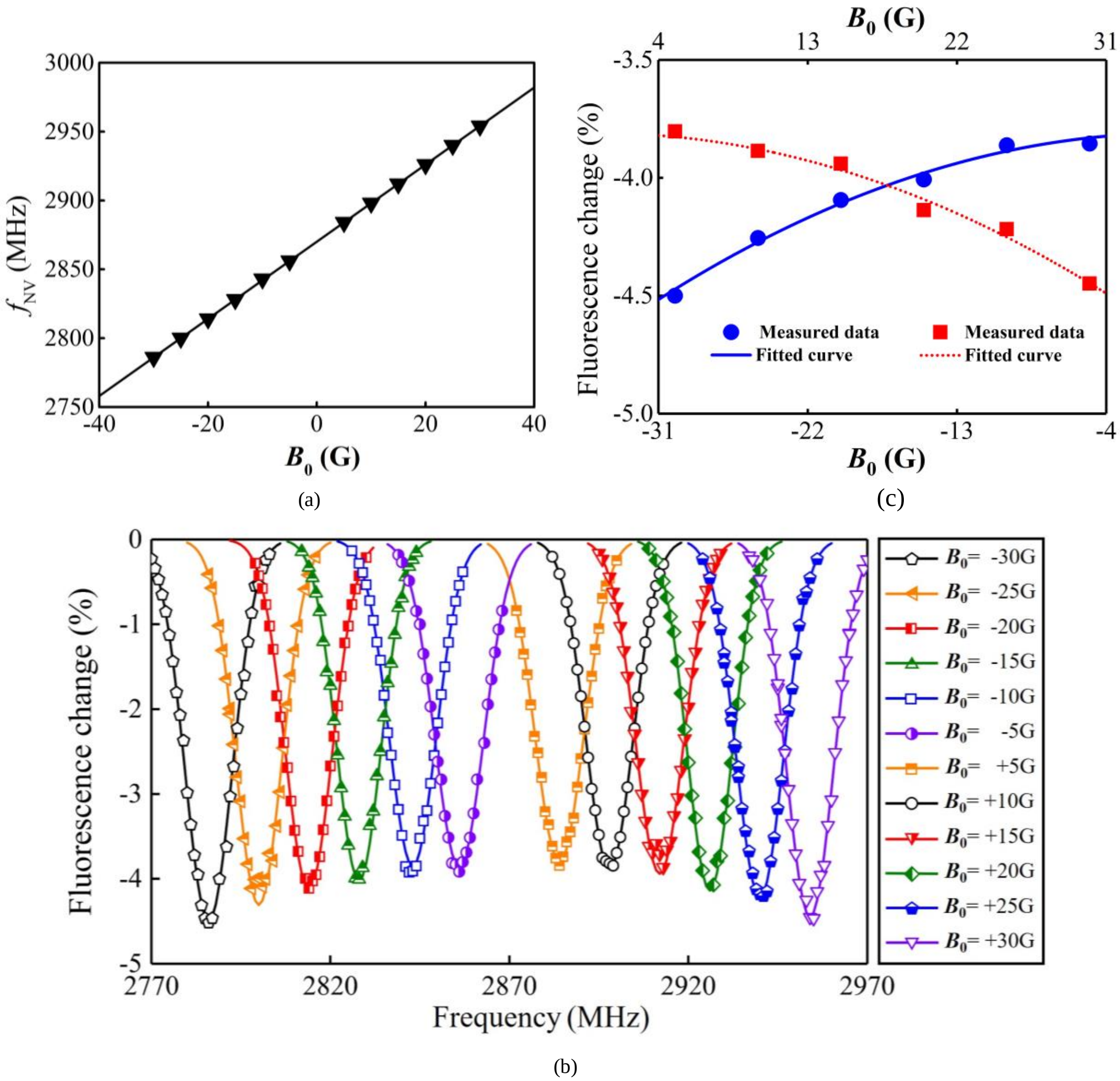

Fig.5. Demonstration of the generation of frequency-tunable MW fields. (a) The f_{NV} as a function of $\boldsymbol{B_0}$. The fitting function is f_{NV} = 2.798 MHz/G × $\boldsymbol{B_0}$ + 2870 MHz. (b) ODMR shifts upon the application of a magnetic field $\boldsymbol{B_0}$ swept in the -30 – +30 G range. The value of $\boldsymbol{B_0}$ is shown in the legend. The scattered data points correspond to the experimental results after averaging 32 sweeps. The curves are fitted with Gaussian functions. (c) Fluorescence contrast (F_{con}) of the resonance peaks as a function of $\boldsymbol{B_0}$. The top and bottom x-axes correspond to the red and blue curves, respectively. The fitting function are F_{con} = 59.18 × exp (-(($\boldsymbol{B_0}$ -0.2896)/285.6)^2) - 62.99.

C. Microwave polarization

To verify that the designed resonator provides circularly polarized MW fields, a magnetic field, ***B***, was applied along the [111] crystal axis. The fluorescence decreases when the MW field and the NV ensemble are in resonance. Four resonance peaks can be observed in the ODMR spectra of the NV ensemble, as shown in Fig. 6. Two external peaks were chosen to observe the effect of the circularly polarized MW fields. The black line indicates the ODMR spectrum for $\Delta\varphi = 0°$, whereas the red and the blues line indicate the ODMR spectra for $\Delta\varphi = 90°$ and $\Delta\varphi = -90°$, respectively.

The Figure 6 clearly shows that the resonator can provide σ+ (σ−) circularly polarized MW fields when $\Delta\varphi = 90°$ (-90°). The electrons of $m_s = 0$ sublevel are excited to $m_s = \pm 1$ sublevels by $\sigma^{\pm}$ circularly polarized MW fields. The changes in the fluorescence detected via the two external resonance peaks produced by the σ+ and σ− circularly polarized MW fields indicate the purity of the MW polarization, which can be expressed as:

$$\rho = (r_+ - r_-)/(r_+ + r_-). \quad (3)$$

Here, $r_{\pm}$ defines the change in the fluorescence corresponding to the $m_S = \pm 1$ sublevels. The calculated purity of the circularly polarized MW, ρ, is 97.17%. These results prove that the resonator provides circularly polarized MW fields by controlling the phase shifter.

By changing the interaction time between the MW field and the electron spin, Rabi oscillations are produced. These results were obtained by calibrating the MW pulse width to excite the electrons to different spin states. When the MW power of the signal generator measures +6 dBm, the Rabi oscillations can be recorded by varying the MW pulse time, T_{MW}, as shown in Fig.

7. The black and blue lines indicate the Rabi oscillations curves for $\Delta\varphi = 0°$ and $\Delta\varphi = -90°$, respectively. Moreover, the Rabi frequency, f_{Rb}, measures 9.26 MHz for $\Delta\varphi = 0°$ and 12.5 MHz for $\Delta\varphi = -90°$. Considering the resonator with different phase difference, the MW pulse width required to excite electrons to different states can ensure the measurement accuracy of the ODMR experiment, which can accurately verify the resonator to provide circularly polarized MW fields.

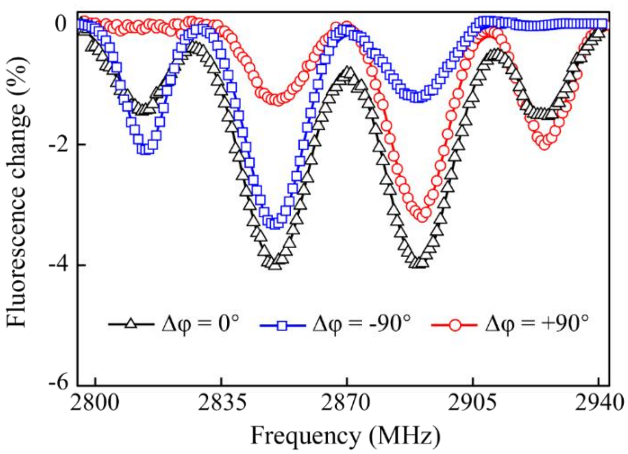

Fig.6. Circularly polarized MW fields. The scattered data points correspond to the experimental results. The curves are fitted by using Gaussian functions.

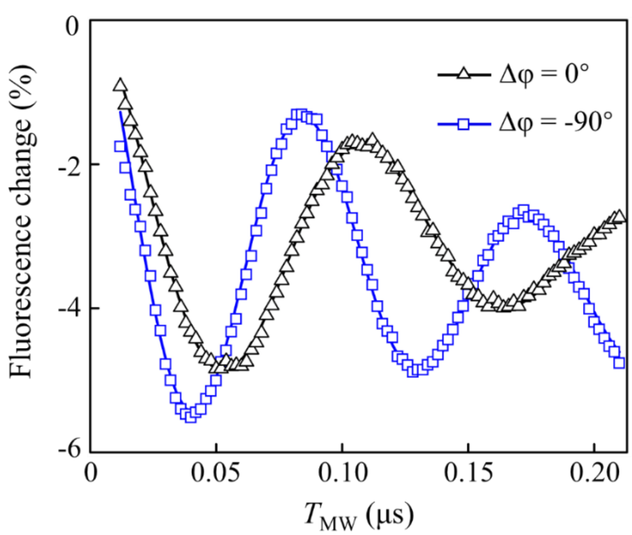

Fig.7. Rabi oscillations. The scattered data points correspond to the experimental results and the solid lines show the fitting curves.

The proposed resonator provides circularly polarized MW fields and the purity of circularly polarized MW is 97.17%. The circularly polarized MW fields release the NV sensing system from the bias magnetic field provided by Helmholtz coils, which makes it useful for miniaturized magnetic field sensors.

IV. Conclusion

In summary, a resonator providing frequency-tunable and circularly polarized MW fields has been demonstrated. The f_{MW} of the resonator is adjustable in the 2.5 ~ 3.1 GHz range by varying the capacitance value of the varactor diode. Moreover, the values of S_{11} corresponding to f_{MW} are lower than -15 dB, ensuring a minimal coupling efficiency of 96.84% between the MW resonator and the MW source. Different values of the external magnetic fields, $\boldsymbol{B}$, are applied to generate a variation in f_{NV} during the ODMR experiment. Upon frequency matching ($f_{MW} = f_{NV}$), the changes in the fluorescence increase with the increase of $|\boldsymbol{B}|$. In addition, the resonator provides a circularly polarized MW signal with a polarization purity of 97.17%. The frequency-tunable and circularly polarized resonator paves the way to further applications and to the development of novel magnetic sensing devices based on diamond NV ensembles.

References

[1] J. Lenz, and A. S. Edelstein, “Magnetic sensors and their applications,” IEEE Sens. J., vol. 6, pp. 631, 2006.
[2] A. Girgin, M. Bilmez, H. Y. Amin, and T. C. Karalar, “A silicon Hall sensor SoC for current sensors,” Microelectron. J., vol. 90, pp. 12, 2019.
[3] P. Ripka, and J. Michal, “Advances in Magnetic Field Sensors,” IEEE Sens. J., vol. 10, pp. 1108, 2010.
[4] G. Govind, N. K. Tiwari, K. K. Agrawal, and M. J. Akhtar, “Microwave imaging of subsurface defects in dielectric structures using complementary split ring resonator,” IEEE Sens. J., vol. 18, pp. 7442, 2018.
[5] J.N. Greiner, D.B.R. Dasari and J. Wrachtrup, “Purification of an unpolarized spin ensemble into entangled singlet pairs,” Sci. Rep., vol. 7, pp. 529, 2017.
[6] J.M. Boss, K.S. Cujia, J. Zopes, and C.L. Degen, “Quantum sensing with arbitrary frequency resolution,” Science, vol. 356, pp. 837, 2017.
[7] C. Zu, W. Wang, L. He, W. Zhang, C. Dai, F. Wang, and L. Duan, “Experimental realization of universal geometric quantum gates with solid-state spins,” Nature, vol. 514, pp. 72, 2014.
[8] S. Arroyo-Camejo, A. Lazariev, S. W. Hell, and G. Balasubramanian, “Room temperature high-fidelity holonomic single-qubit gate on a solid-state spin,” Nat. Commun., vol. 5, pp. 4870, 2014.
[9] Y. Sekiguchi, Y. Komura, S. Mishima, T. Tanaka, N. Niikura, and H. Kosaka, “Geometric spin echo under zero field,” Nat. Commun., vol. 7, pp. 11668, 2016.
[10] G. Bian, H. Yuan, N. Zhang, L. Xu, J. Zhang, P. Fan, H. Wang, C. Zhang, G. Shan, Q. Zhang, and J. Fang, “Neutral oxygen-vacancy defect in cubic boron nitride: A plausible qubit candidate,” Appl. Phys. Lett., vol. 114, pp. 102105, 2019.
[11] G. Waldherr, Y. Wang, S. Zaiser, M. Jamali, T. Schulte-Herbrüggen, H. Abe, T. Ohshima, J. Isoya, J. F. Du, P. Neumann, and J. Wrachtrup, “Quantum error correction in a solid-state hybrid spin register,” Nature, vol. 506, pp. 204, 2014.
[12] N. Zhang, C. Zhang, L. Xu, M. Ding, W. Quan, Z. Tang, and H. Yuan, “Microwave magnetic field coupling with nitrogen vacancy center ensembles in diamond with high homogeneity,” Appl. Magn. Reson., vol. 47, pp. 589, 2016.
[13] N. Zhang, H. Yuan, C. Zhang, L. Xu, J. Zhang, G. Bian, P. Fan, H. Yuan, and J. Fang, “Microwave field uniformity impact on dc magnetic sensing with NV ensembles in diamond,” IEEE Sens. J., vol. 19, pp. 451, 2019.
[14] S. Sangtawesin, T. O. Brundage, Z. J. Atkins, and J. R. Petta, “Highly tunable formation of nitrogen-vacancy centers via ion implantation,” Appl. Phys. Lett., vol. 105, pp. 063107, 2014.

[15] T. Shimo-Oka, H. Kato, S. Yamasaki, F. Jelezko, S. Miwa, Y. Suzuki, and N. Mizuochi, "Control of coherence among the spins of a single electron and the three nearest neighbor {sup 13}C nuclei of a nitrogen-vacancy center in diamond," Appl. Phys. Lett., vol. 106, pp. 153103, 2015.

[16] S. Ahmadi, H. A. R. El-Ella, J. B. Hansen, A. Huck, and U. L. Andersen, "Pump-enhanced continuous wave magnetometry using nitrogen-vacancy ensembles," Phys. Rev. Appl., vol. 10, pp. 034001, 2017.

[17] P. Wang, Z. Yuan, P. Huang, X. Rong, M. Wang, X. Xu, C. Duan, C. Ju, F. Shi, and J. Du, "High-resolution vector microwave magnetometry based on solid-state spins in diamond," Nat. Commun., vol. 6, pp. 6631, 2015.

[18] B. J. Maertz, A. P.Wijnheijmer, G. D. Fuchs, M. E. Nowakowski, and D. D. Awschalom, "Vector magnetic field microscopy using nitrogen vacancy centers in diamond," Appl. Phys. Lett., vol. 96, pp. 092504, 2010.

[19] J. M. Taylor, P. Cappellaro, L. Childress, L. Jiang, D. Budker, P. R. Hemmer, A. Yacoby, R. Walsworth, and M. D. Lukin, "High-sensitivity diamond magnetometer with nanoscale resolution," Nat. Phys., vol. 4, pp. 810, 2008.

[20] R. L. Fagaly, "Superconducting quantum interference device instruments and applications," Rev. Sci. Instr., vol. 77, pp. 101101, 2006.

[21] J. C. Allred, R. N. Lyman, T. W. Kornack, and M. V. Romalis, "High-sensitivity atomic magnetometer unaffected by spin-exchange relaxation," Phys. Rev. Lett., vol. 89, pp. 130801, 2002.

[22] I. K. Kominis, T. W. Kornack, J. C. Allred, and M. V. Romalis, "A subfemtotesla multichannel atomic magnetometer," Nature, vol. 422, pp. 596, 2003.

[23] C. Zhang, H. Yuan, Z. Tang, W. Quan, and J. Fang, "Inertial rotation measurement with atomic spins: From angular momentum conservation to quantum phase theory," Appl. Phys. Rev., vol. 3, pp. 041305, 2016.

[24] C. Zhang, H. Yuan, N. Zhang, L. Xu, J. Zhang, B. Li, and J. Fang, "Vector magnetometer based on synchronous manipulation of nitrogen-vacancy centers in all crystal directions," J. Phys. D: Appl. Phys., vol. 51, pp.155102, 2018.

[25] J. Mu, Q. Z, Z. Ma, S. Zhang, Y. Shi, J. Gao, X. Zhang, H. Cao, L. Qin, J. Liu, and Y. Li, "Ensemble spin fabrication and manipulation of NV centres for magnetic sensing in diamond," Sens. Rev., vol. 37, pp. 419, 2017.

[26] T. Wolf, P. Neumann, K. Nakamura, H. Sumiya, T. Ohshima, J. Isoya, and J. Wrachtrup, "Subpicotesla Diamond Magnetometry," Phys. Rev. X, vol. 5, pp. 041001, 2015.

[27] T. P. M. Alegre, C. Santori, G. Medeiros-Ribeiro, R. G. Beausoleil, "Polarization-selective excitation of nitrogen vacancy centers in diamond," Phys. Rev. B, vol. 76, pp. 165205, 2007.

[28] E. Abe, and K. Sasaki, "Tutorial: Magnetic resonance with nitrogen-vacancy centers in diamond-microwave engineering, materials science, and magnetometry," J. Appl. Phys., vol. 123, pp. 161101, 2018.

[29] H. Zheng, J. Xu, G. Z. Iwata, T. Lenz, J. Michl, B. Yavkin, K. Nakamura, H. Sumiya, T. Ohshima, J. Isoya, J. Wrachtrup, A. Wickenbrock, and D. Budker, "Zero-field magnetometry based on nitrogen-vacancy ensembles in diamond," Phys. Rev. Appl., vol. 11, pp. 064068, 2019.

[30] X. Yang, N. Zhang, H. Yuan, G. Bian, P. Fan, and M. Li, "Microstrip-line resonator with broadband, circularly polarized, uniform microwave field for nitrogen vacancy center ensembles in diamond," AIP Adv., vol. 9, pp. 075213, 2019.

[31] T. P. M. Alegre, A. C.Torrezan, and G. Medeiros-Ribeiro, "Microstrip resonator for circularly polarized microwaves," Appl. Phys. Lett., vol. 91, pp. 204103, 2007.

[32] M. Mrozek, J. Mlynarczyk, D. S. Rudnicki, and W. Gawlik, "Circularly polarized microwaves for magnetic resonance study in the GHz range: Application to nitrogen-vacancy in diamonds," Appl. Phys. Lett., vol. 107, pp. 013505, 2015.

[33] N. Zhang, H. Yuan, C. Zhang, L. Xu, J. Zhang, G. Bian, B. Li, and J. Fang, "Robust frequency calibration of a large-area highQ resonator in magnetic imaging with spin ensembles in diamond," Appl. Phys. Express, vol. 11, pp. 086602, 2018.

[34] L. Xu, H. Yuan, N. Zhang, J. Zhang, G. Bian, P. Fan, M. Li, C. Zhang, Y. Zhai, and J. Fang, "High-efficiency fluorescence collection for NV center ensembles in diamond," Opt. Express, vol. 27, pp. 358960, 2019.

[35] V. Stepanov, F. H. Cho, C. Abeywardana, and S. Takahashi, "High-frequency and high-field optically detected magnetic resonance of nitrogen-vacancy centers in diamond," Appl. Phys. Lett., vol. 106, pp. 063111, 2015.

Heng Yuan is currently Assoc. Professor at the School of Instrument Science and Opto-Electronic Engineering Beihang University, and Key Laboratory of Ministry of Industry and Information Technology on Quantum Sensing Technology, Beijing, China. His research fields are pH Sensors, Biosensors, Spintronic Device, and Quantum Precision Measurement.

Xiaoying Yang received the bachelor's degree from the school of mechanical and electronic engineering, Wuhan University of Technology, China, in 2017. She is currently pursuing the master's degree at the School of Instrumentation Science and Opto-electronics Engineering, Beihang University, Beijing, China. Her main research interests include the design of microwave components and magnetic sensors.

Ning Zhang received her bachelor's degree in School of Astronautics, Beihang University, China in 2012. She is currently Ph.D. candidate in School of Instrumentation and Opto-electronics Engineering, Beihang University, China. Her research includes Solid-state Spin Materials, Microwave Sensors, Temperature Sensors and Magnetic Sensors.

Zhiqiang Han received the bachelor's degree from the school of Beihang University, China, in 2018. He is currently pursuing the master's degree at the School of Instrumentation Science and Opto-electronics Engineering, Beihang University, Beijing, China. His main research interests include the design of magnetic sensors.

Lixia Xu received her bachelor's degree in College of Instrumentation and Electrical Engineering, Jilin University, Jilin in 2014. She is Ph.D. candidate in School of Instrumentation Science and Opto-Electronics Engineering, Beihang University, Beijing, China. Her research activities include Quantum Sensors.

Jixing Zhang received his bachelor's degree in school of instrumentation
Science and Opto-Electronics Engineering, Beihang University, Beijing, in 2016. He is currently Ph.D. candidate in School of Instrumentation Science and Opto-Electronics Engineering, Beihang University, Beijing, China. His research activities include Quantum Sensors.

Guodong Bian received his bachelor's degree in School of Physics, Shandong University, Shandong in 2016. He is currently Ph.D. candidate in School of Instrumentation Science and Opto-Electronics Engineering , Beihang University, Beijing, China. His research activities include Quantum Sensors and Quantum Information Processing.

Pengcheng Fan received his bachelor's degree of Applied Physics in Department of Physics from Beijing Institute of Technology, Beijing in 2015. He is currently Ph.D. candidate in School of Instrumentation Science and OptoElectronics Engineering, Beihang University, Beijing, China. His research interests include MEMS Sensors and Quantum Sensors.

Mingxin Li received the bachelor's degree in School of Automation, Northwestern Polytechnical University, Shanxi province, in 2017. He is currently pursuing the Ph.D. degree with the School of Instrumentation Science and Opto-electronics Engineering, Beihang University, Beijing, China. His research interests include quantum sensors and quantum information.

Yuchen Liu received the bachelor's degree from the School of mechanical and electronic engineering, Qingdao University, China, in 2018. He is currently pursuing the Ph.D. degree with the School of Instrumentation Science and Opto-electronics Engineering, Beihang University, Beijing. His research interests include hardware design and quantum sensors.